Materials Science & Engineering A 836 (2022) 142720

Contents lists available at ScienceDirect

Materials Science & Engineering A

journal homepage: www.elsevier.com/locate/msea

Outstanding cryogenic strength-ductility properties of a cold-rolled medium-entropy TRIP $Fe_{65}(CoNi)_{25}Cr_{9.5}C_{0.5}$ alloy

E. Povolyaeva, S. Mironov, D. Shaysultanov *, N. Stepanov, S. Zherebtsov

Belgorod National Research University, 85 Pobeda Str, 308015, Belgorod, Russian Federation

ARTICLE INFO

Keywords:
Medium-entropy alloys
Cryogenic temperature
Strain hardening
Martensitic transformation
Transformation-induced plasticity

ABSTRACT

A new medium-entropy $Fe_{65}(CoNi)_{25}Cr_{9.5}C_{0.5}$ (at.%) alloy was investigated both at room and liquid nitrogen temperatures in both the as-cast and deformed conditions. The deformed sample was obtained by cold rolling the alloy until a thickness reduction of 80% had been reached. During testing at −196 °C, the cold-rolled program alloy exhibited a combination of very high strength ($\sigma_{0.2}$ = 1360 MPa, σ_{UTS} = 2070 MPa), good ductility (δ = 26%) and excellent fracture toughness (approximately 700 kJ/m^2). Examination of the microstructure suggested a deformation-induced phase transition from the initial face-centered cubic (fcc) phase to the martensite body-centered cubic (bcc) phase. The enhanced mechanical properties of the cold-rolled alloy at cryogenic temperatures, in comparison with the as-cast alloy, could be associated with an increased thermal stability of the fcc phase caused by deformation-induced microstructure refinement and shifting of the main martensite transformation to later stages of strain. Substructure strengthening, interphase strengthening, and solid solution strengthening could also contribute to the high strength and good ductility of the alloy. The obtained results can expand the possibilities for the development of medium-entropy ferrous alloys for use at extremely low temperatures.

1. Introduction

The development of multicomponent alloys with a close to equiatomic content of elements (high-entropy or medium-entropy alloys (HEAs or MEAs, respectively)) has attracted great interest because of the vast composition space, which opens the possibility of creating metallic materials with a unique combination of exceptional properties. Among many options, HEAs and MEAs with twinning-induced plasticity/transformation-induced plasticity (TWIP/TRIP) effects possess significant strain hardening and, therefore, demonstrate a good combination of strength and ductility. In some cases, decreasing the temperature to cryogenic conditions even improves their mechanical properties [1–7], which makes these materials attractive for low-temperature and cryogenic applications.

The TRIP effect is usually associated with a decreased stability of the face-centered cubic (fcc) phase. It is well known that the TRIP effect is not observed in HEAs with a relatively stable fcc phase (similar to equiatomic CoCrFeMnNi [8,9]). Meanwhile, in some alloys with a higher Fe content, the fcc phase can become unstable, and a larger fraction of Fe decreases the cost of the alloy. For example, good strength-ductility properties were reported for $Fe_{50}Mn_{30}Co_{10}Cr_{10}$ (hereinafter, the compositions are given in at.%) alloy [10], in which the hcp ε-martensite was formed during deformation. Later, $Fe_{60}(CoNi)_{30}Cr_{10}$ and $Fe_{65}Co_{10}Ni_{10}Cr_{15}$ medium-entropy alloys with a higher fraction of iron have been proposed [1,6]. Owing to the deformation-induced fcc-to-bcc phase transformation, these alloys showed a good balance of strength (up to approximately 1.5 GPa) and ductility (up to 87%) at 77 K. A more detailed study of the $Fe_{60}Co_{15}Ni_{15}Cr_{10}$ alloy suggests that unusual mechanical properties during cryogenic deformation can be associated with a relatively high strain rate sensitivity and low activation volume [5]. Interstitial elements such as C can also strongly affect the fcc phase stability; in addition, carbon promotes additional strengthening mechanisms such as interstitial solid solution strengthening and/or precipitation hardening [2,11–13].

However, the phase stability and associated mechanical performance of the alloys can depend not only on their chemical composition, but also on their microstructure. For example, in Ref. [14], it was revealed that at the same fcc/hcp phase ratio, strength and ductility were enhanced simultaneously in the $Fe_{50}Mn_{30}Co_{10}Cr_{10}$ alloy with decreasing fcc grain size because of the higher stability of the fcc phase. Similar results, that

* Corresponding author.
E-mail address: shaysultanov@bsu.edu.ru (D. Shaysultanov).

https://doi.org/10.1016/j.msea.2022.142720
Received 27 October 2021; Received in revised form 21 January 2022; Accepted 22 January 2022
Available online 24 January 2022

is, simultaneous improvement of strength and ductility, were reported for the $Fe_{42}Mn_{28}Co_{10}Cr_{15}Si_5$ alloy after friction stir processing [15], where enhanced mechanical performance was also attributed to the increased metastability of a finer-grained fcc phase.

However, the effect of microstructure on the mechanical behavior of Fe-rich TRIP HEAs/MEAs is still not sufficiently understood. For example, the introduction of various lattice defects during cold working can also affect the stability of the fcc phase [16], but most studies (e.g., mentioned above) on TRIP HEAs/MEAs have focused on well-recrystallized alloys. In the present work, the mechanical behavior of a new $Fe_{65}(CoNi)_{30}Cr_{9.5}C_{0.5}$ medium entropy alloy in as-cast and cold-worked conditions was examined. The superior cryogenic mechanical properties of the cold-worked alloy were unexpectedly revealed.

2. Materials and methods

Non-equiatomic $Fe_{65}(CoNi)_{25}Cr_{9.5}C_{0.5}$ alloy (subscripts correspond to the concentration of elements in at.%) was obtained from mixtures of pure (≥99.9%) constitutive elements by vacuum induction melting. The configurational entropy of the alloy was 1.05R, which corresponds to the definition of an MEA [17]. The produced ingots had a nearly rectangular shape, measuring 80 × 80 × 25 mm^3. The measured composition of the alloy (determined using optical emission spectroscopy or energy dispersive spectrometry (EDS); the percentages of C, S, P, and N were determined by LECO thermal combustion analysis) are shown in Table 1.

Specimens for cold rolling, microstructure analysis, and mechanical testing were cut from the as-cast ingots using an electric discharge machine. Samples measuring 60 × 30 × 25 mm^3 were cold-rolled at room temperature. Unidirectional multipass rolling to a total thickness strain of 80% (from 25 to 5 mm) was performed using a reduction per pass of 3–5%.

The microstructure of the alloy was studied using a Nova NanoSEM scanning electron microscope (SEM) with a backscattered electron (BSE) detector and an electron backscattering diffraction (EBSD) camera and using a transmission electron microscope (TEM) (JEOL JEM-2100) equipped with an EDS detector. Although both body-centered cubic (bcc) α and body-centered tetragonal (bct) α martensite have been reported to form from the face-centered cubic (fcc) γ austenite in various metals [18,19], during EBSD mapping, the martensitic phase was indexed as a body-centered cubic phase, similar to that observed in the $Fe_{60}(CoNi)_{30}Cr_{10}$ alloy [1].

To study the microstructure using TEM, the samples were mechanically thinned to 100 μm, and the resulting foils were subjected to conventional two-jet electropolishing in a mixture of 90% CH_3COOH and 10% $HClO_4$ at a voltage of 30 V at room temperature. X-ray diffraction analysis (XRD) was performed on an ARL-X'tra diffractometer (Thermo Fisher Scientific, Portland, Oregon, USA) with Cu-Kα radiation.

Tensile tests of dog-bone flat specimens (gage size 12 × 3 × 1.5 mm^3) were performed at room and cryogenic temperatures using an Instron 5882 universal testing machine with an initial strain rate of 10^{-3} s^{-1}. The fracture toughness tests were carried out at room and cryogenic temperatures on an Instron IMP460 pendulum impact machine using Charpy V-notch specimens measuring 55 × 8 × 2 mm^3. At least three specimens were tested per condition.

3. Results

The IPF and phase maps of the as-cast and cold-rolled (CR) $Fe_{65}(CoNi)_{25}Cr_{9.5}C_{0.5}$ MEAs are shown in Fig. 1. The EBSD phase composition maps suggest that the alloy in the as-cast condition comprises approximately 65% of the fcc matrix phase (Fig. 1a and b, Table 2) and "islands" of the bcc phase (approximately 35%). The lamellar morphology of the bcc phase suggests the martensitic mechanism of this phase formation, in contrast to the high-temperature δ phase, which forms in some steels during crystallization [20]. The average sizes of the fcc and bcc particles were found to be 390 μm and 23 μm, respectively. The pole figure analysis suggests the existence of an orientation relationship (OR) between the fcc and bcc phases in the initial condition; however, it was quite difficult to assign only one OR because signs of both Kurdjumov-Sachs and Nishiyama-Wassermann ORs could be found (Supplementary Fig. S1). The "mixture" of orientation relationships could be caused by high internals stresses in the martensitic phase as well as the relative proximity of the main ORs between bcc and fcc lattices [21].

Cold rolling led to noticeable grain elongation and the formation of deformation bands inclined at approximately 45°from the rolling direction (Fig. 1c). The percentage of the bcc phase increased by approximately 10% in comparison with the as-cast state (Fig. 1d, Table 2), because the fcc phase could no longer be considered as the phase matrix.

Bright-field TEM images show that the alloy in both conditions has a two-phase fcc + bcc structure (Fig. 2 a and b); no signs of carbide particles were detected. Dislocation pile-ups and individual dislocations could be recognized in both phases of the as-cast condition (Fig. 2a). Cold rolling to a thickness reduction of 80% resulted in the formation of a lamellar structure comprising alternating fcc and bcc laths; the latter most probably was formed as a result of the fcc-to-bcc martensite transformation. The dislocation densities in the lamellae of both phases were very high.

The mechanical behavior of the alloy was found to be quite different depending on the conditions and testing temperature. At room temperature (Fig. 3a), the as-cast condition of the alloy showed an extensive strain hardening stage, resulting in almost four times higher ultimate tensile strength in comparison with the yield strength (Table 3) and considerable uniform elongation. After cold rolling, the mechanical behavior of the alloy was typical of largely strained materials: high strength, early necking, and low ductility (Fig. 3a, Table 3). A decrease in the testing temperature to −196 °C resulted in a considerable increase in the yield strength under both conditions of the alloy (Fig. 3b, Table 3). The strain-hardening stage of the alloy became shorter in the as-cast condition at cryogenic temperatures, while after cold rolling, the alloy surprisingly demonstrated a long strain-hardening stage. Thus, the alloy in the CR condition had a high ultimate tensile strength (above 2 GPa) and good elongation (approximately 26%).

The strain hardening of the alloy reflected its mechanical behavior. In the as-cast condition, the alloy showed a stable (albeit low) strain hardening rate at room temperature (Fig. 3c). At cryogenic temperatures, the initially rather high strain-hardening rate rapidly decreased with strain (Fig. 3d). A very fast drop in the $d\sigma/d\varepsilon$ value was observed for the cold-rolled alloy tensioned at room temperature (Fig. 3c). The high strain hardening rate surprisingly increased by approximately 40% at $\varepsilon \sim 0.1$ during testing under the same conditions at −196 °C before decreasing to zero at $\varepsilon \sim 0.2$ (Fig. 3d).

Table 1
Chemical composition of the program alloys.

Composition	Fe	Co	Ni	Cr	C	Si	Mn	Cu	Al	Ti	P	S	N
Nominal (at.%)	65.0	12.5	12.5	9.5	0.5	–	–	–	–	–	–	–	–
Actual (at. %)	64.92	12.44	12.49	9.43	0.51	0.14	0.01	0.01	0.04	0.001	0.003	0.005	0.008
Actual (wt.%)	64.81	13.10	13.10	8.76	0.11	0.07	0.01	0.01	0.019	0.001	0.002	0.003	0.002

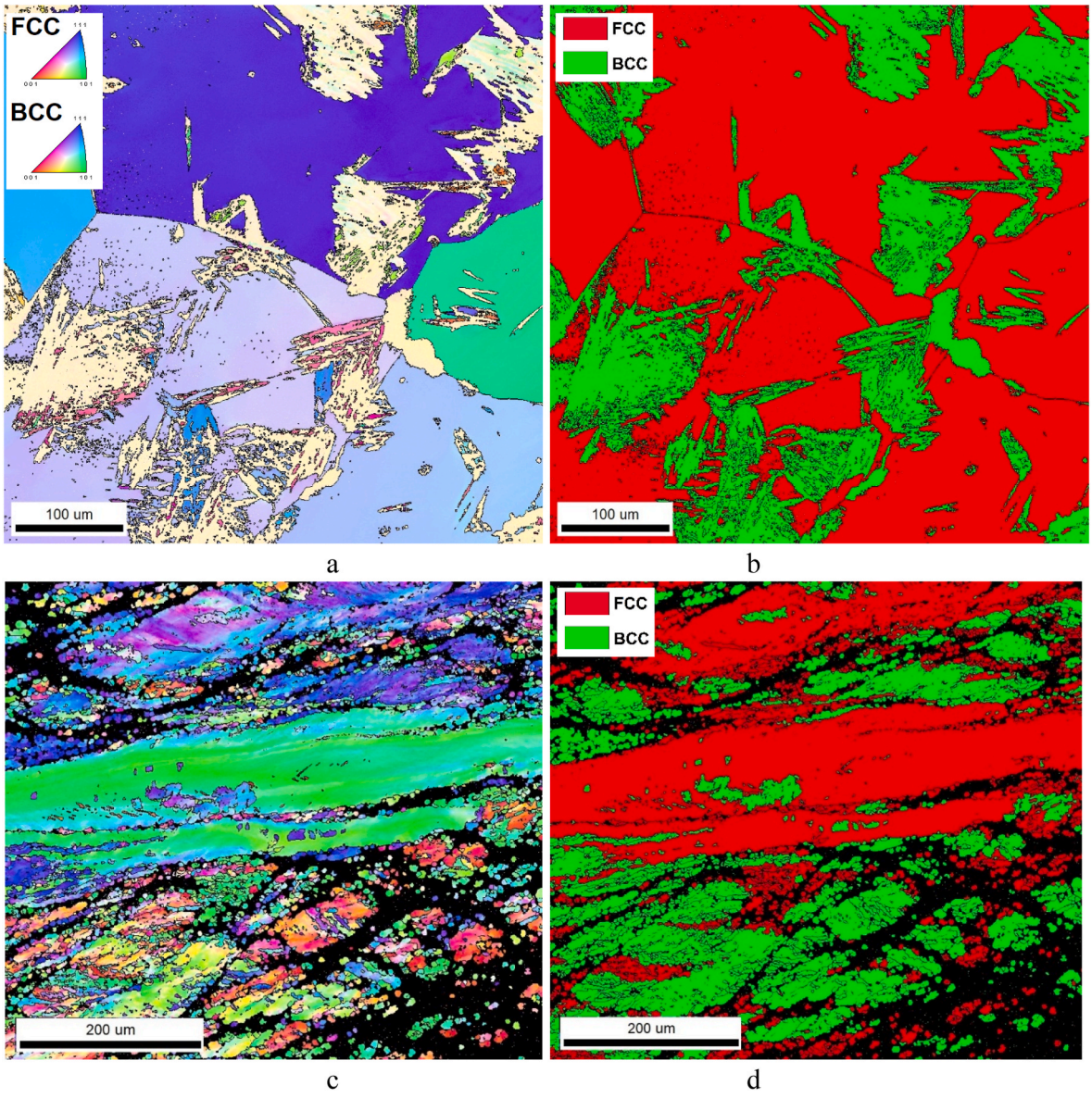

Fig. 1. IPF (a, c) and phase (b, d) maps of the as-cast (a, b) or CR to 80% (c, d) $Fe_{65}(CoNi)_{25}Cr_{9.5}C_{0.5}$ alloy.

Table 2
Phase composition of the $Fe_{65}(CoNi)_{25}Cr_{9.5}C_{0.5}$ alloy in the various conditions.

Condition	Volume fraction, %	
	Bcc	fcc
As-cast	34.6	65.4
As-cast tensioned at 25 °C	46.3	49.7
As-cast tensioned at −196 °C	93.9	6.1
Cold rolled (CR) to 80%	43.2	56.8
CR tensioned at 25 °C	46.5	53.5
CR tensioned at −196 °C	99.7	0.3

The fracture toughness of the alloy (Table 4) correlates well with the tensile test results. The as-cast condition of the alloy during the Charpy V-notch impact test at room temperature showed the maximum value of fracture toughness (980 kJ/m^2), while the cold-rolling condition had the minimum value (640 kJ/m^2). At cryogenic temperatures, the ductile as-cast condition had a somewhat higher value of fracture toughness (860 kJ/m^2) compared to that of the cold-rolled condition (700 kJ/m^2).

To gain insight into the mechanism of the observed deformation behavior of the alloy, EBSD investigation of the specimens after tensile tests was performed (Fig. 4). The as-cast condition tensioned at room temperature (Fig. 4 a, b) comprised two phases, that is, fcc and bcc; the fraction of the martensitic bcc phase increased to approximately 46% (Table 2). The presence of boundaries that were nearly parallel to the {111} plane traces and clustering of the rotation axes of the 55-63° boundaries near <111> suggested the development of mechanical twinning (Supplementary Figs. S2 and S3). In addition, a lamellar substructure with a misorientation between lamellae of 1.5–2° (Supplementary Fig. S4) can be observed in the fcc phase. The bcc phase had a typical elongated martensite structure comprising packs of martensitic lamellae (Fig. 4b).

Tension to fracture of the cold-rolled specimen resulted in the formation of crossing localized deformation bands in both phases (Fig. 4 c, d). In addition, a rather high fraction of the twin boundaries (Supplementary Figs. S2 and S3) could also be observed in the fcc phase. The percentage of the bcc phase changed only slightly after the tensile test (Table 2).

A decrease in the testing temperature to −196 °C resulted in a considerable change in the microstructure after tension to fracture

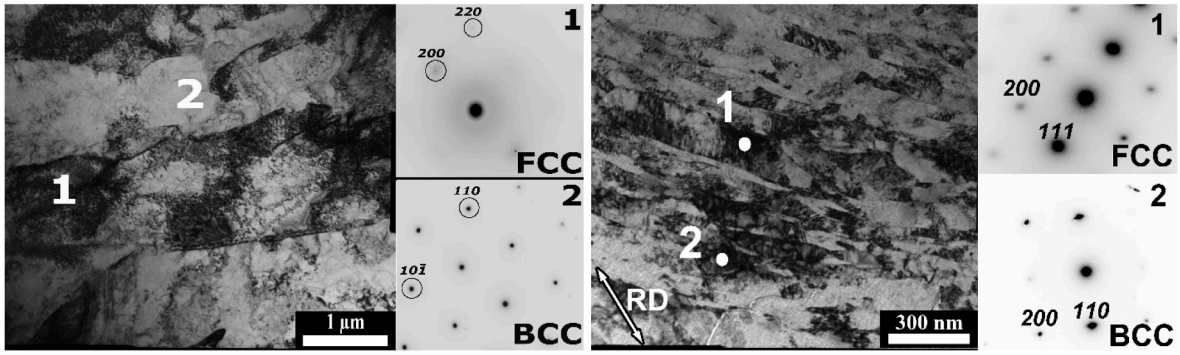

Fig. 2. Bright-field TEM images of the as-cast (a) and CR to 80% (b) $Fe_{65}(CoNi)_{25}Cr_{9.5}C_{0.5}$ alloy.

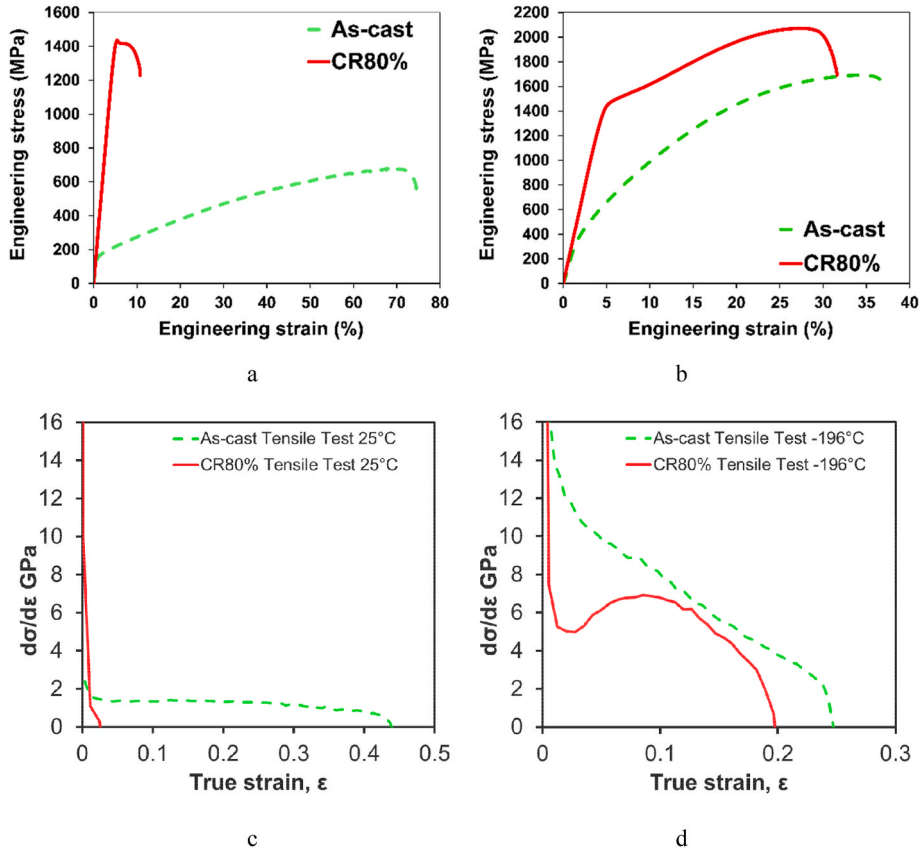

Fig. 3. Representative tensile stress-strain (a,b) and strain hardening (c,d) curves of the as-cast or CR to 80% $Fe_{65}(CoNi)_{25}Cr_{9.5}C_{0.5}$ alloy obtained at room (a,c) or cryogenic (b,d) temperatures.

Table 3
Mechanical properties of the $Fe_{65}(CoNi)_{25}Cr_{9.5}C_{0.5}$ alloy obtained during tensile tests at room or cryogenic temperatures.

Testing temperature, °C	Condition	$\sigma_{0.2}$, MPa	σ_{UTS}, MPa	δ, %
20	As-cast	155 ± 10	680 ± 20	65 ± 3
	CR 80%	1385 ± 25	1440 ± 35	6 ± 1
−196	As-cast	375 ± 15	1690 ± 30	27 ± 2
	CR 80%	1380 ± 30	2070 ± 35	26 ± 2

Table 4
Charpy V-notch impact energy and fracture toughness of the $Fe_{65}(CoNi)_{25}Cr_{9.5}C_{0.5}$ alloy obtained at room or cryogenic temperatures.

Testing temperature, °C	Condition	Fracture toughness, kJ/m^2	Charpy V-notch impact energy, J
25	As-cast	980 ± 55	13.5 ± 0.3
	CR80%	640 ± 25	6.5 ± 0.1
−196	As-cast	860 ± 45	13.7 ± 0.3
	CR80%	700 ± 30	6.2 ± 0.2

(Fig. 5). The microstructure in the as-cast condition during deformation at cryogenic temperature almost completely transformed into bcc lamellar martensite with only 3% of the fcc phase (Fig. 5b).

The cold-rolled alloy also showed almost complete transformation of the fcc phase into bcc during the tension test at −196 °C (Fig. 5d). The fraction of the reliably determined fcc phase was found to be only 0.3%. The martensite lamellae in some places (the central part of Fig. 5 c and

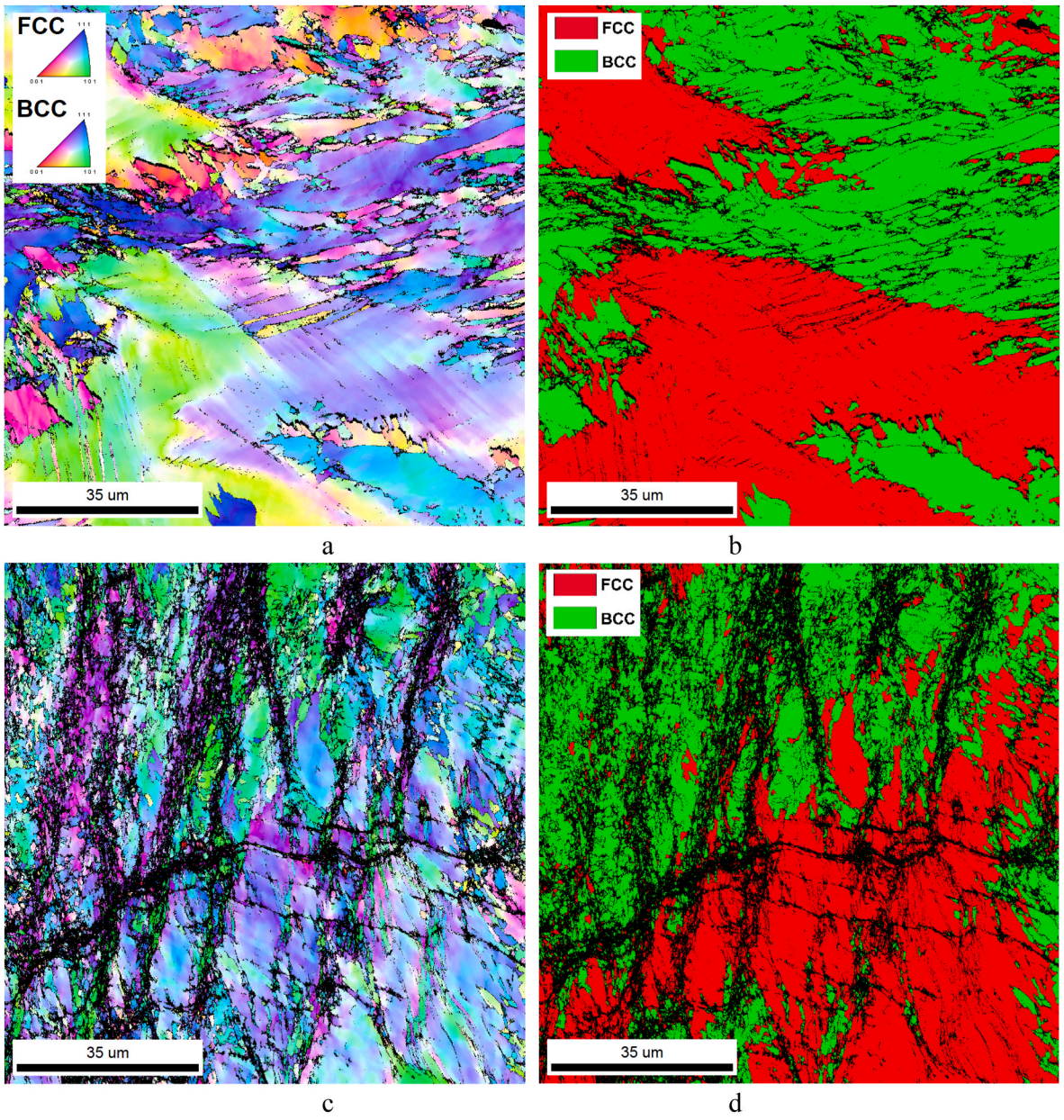

Fig. 4. IPF (a, c) and phase (b, d) maps of the as-cast (a, b) or CR to 80% (c, d) $Fe_{65}(CoNi)_{25}Cr_{9.5}C_{0.5}$ alloy after tension to fracture at room temperature.

d) were fragmented due to deformation. It should be noted, however, that in both cases the presence (Fig. 5b,d) of the bcc phase in large, nearly equiaxial areas, without typical martensitic structure lamellar morphology, was observed.

4. Discussion

The obtained results showed very high mechanical properties of the deformed $Fe_{65}(CoNi)_{25}Cr_{9.5}C_{0.5}$ alloy at cryogenic temperatures. Specifically, during testing at −196 °C, the alloy cold rolled to 80% thickness reduction demonstrated a combination of very high strength ($\sigma_{0.2}$ = 1360 MPa, σ_B = 2070 MPa), good ductility (δ = 26%), and a Charpy fracture toughness of 700 kJ/m^2. Moreover, the cryogenic strength of the as-cast alloy substantially increased after cold working without noticeable sacrifice in ductility and toughness (Tables 3 and 4).

These characteristics could be ascribed to the superposition of several strengthening mechanisms. The most obvious mechanism causing the increase in both strength and ductility was the fcc-to-bcc martensitic transformation. For example, the deformation of the as-cast alloy at room temperature resulted in considerable strengthening (more than four times) owing to the fcc-to-bcc transformation (Fig. 3a and Table 2). It should be noted that the martensite formation and corresponding interface strengthening could result in the enhancement of both strength and ductility depending on the interphase nature (coherent, semi-coherent, or incoherent). As suggested by Bae et al. [1], coherent fcc-bcc interfaces can increase ductility owing to the generation of a large number of dislocations during lattice volume expansion, while semi-coherent or incoherent fcc-bcc interfaces contribute to strengthening.

The fraction of the bcc phase in the initial as-cast condition was approximately 34%, thereby suggesting that the M_s temperature was well above 25 °C. A crude evaluation of M_s using relations proposed by Jaffe and Hollomon [22], Kobayashi et al. [23], and Zhao [24] showed that the martensite transformation in the program alloy could start in the interval of approximately 300–500 °C, resulting in a large amount of martensite in the microstructure at room temperature. It is worth noting

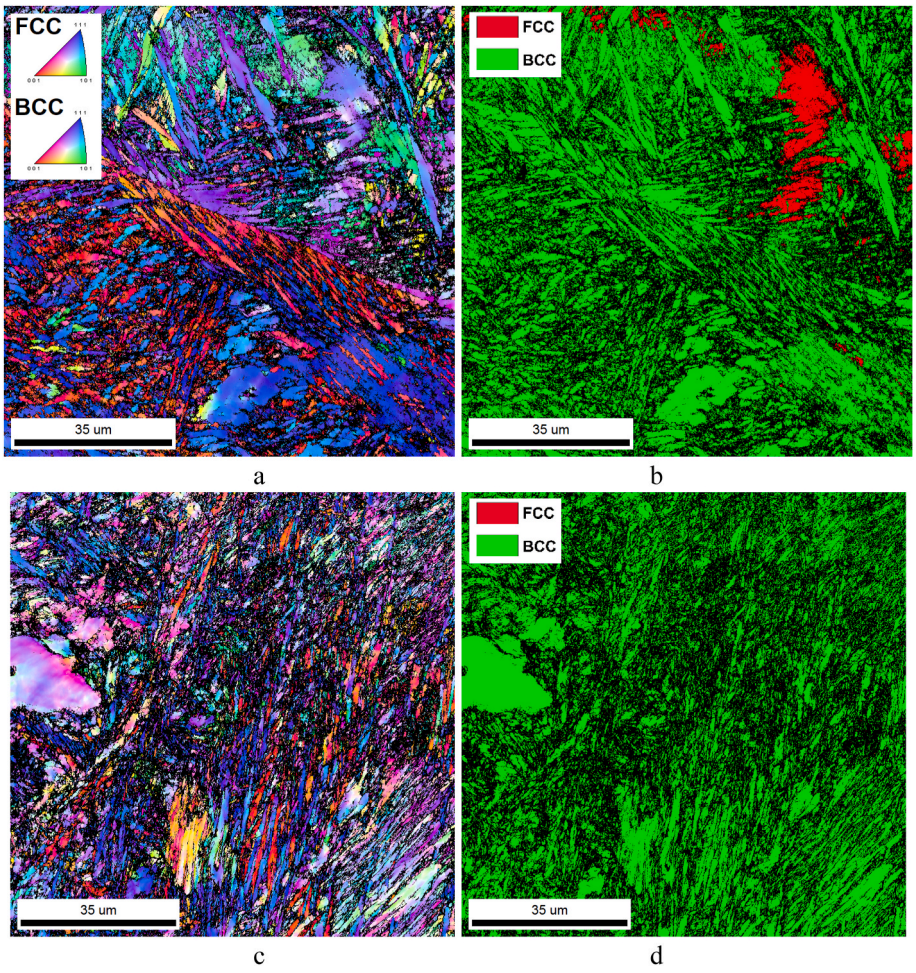

Fig. 5. IPF (a, c) and phase (b, d) maps of the as-cast (a, b) or CR to 80% (c, d) $Fe_{65}(CoNi)_{25}Cr_{9.5}C_{0.5}$ alloy after tension at −196 °C.

that some additional contribution to the fcc phase stability could also be expected due to the presence of carbon [25] when compared with similar carbon-free MEAs [6], where the fraction of bcc was 7% in the recrystallized condition.

Further straining at room temperature increased the fraction of martensite; however, the maximum amount of the bcc phase at room temperature did not exceed 47% even after a very high deformation level (approximately 43% of bcc after 80% CR and approximately 46% after tension tests under both conditions of the alloys (as-cast and 80% CR). Owing to the relatively low fraction of deformation-induced martensite, the mechanical behavior of the $Fe_{65}(CoNi)_{25}Cr_{9.5}C_{0.5}$ alloy in the as-cast condition showed limited signs of TRIP, that is, rather high total elongation (65%) and relatively stable strain hardening rate up to $\varepsilon \sim 0.45$ (Fig. 3a,c, Table 2). This behavior was most likely associated with the formation of deformation-induced martensite, as the net sum of the bcc phase increased from 34.6% to 46.3%. If almost all the martensite formed during previous cold rolling (43.2% of bcc after 80% CR), further tension did not result in a noticeable TRIP effect, and the alloy behaved like a typical largely deformed metallic material with high strength and very low uniform and total elongation (Fig. 3a,c, Table 2).

A decrease in temperature influenced the mechanical behavior of the alloy in the as-cast and deformed conditions differently. Specifically, the as-cast alloy demonstrated a yield point that was more than twice as high as that obtained during room-temperature tests (375 MPa *vs.* 155 MPa; Table 2). This difference became even more pronounced during deformation because the alloy attained a σ_{UTS} of approximately 1700 MPa. At the same time, the ductility of the alloy decreased at cryogenic temperatures by more than two times to 27% (Fig. 3 a,b, Table 2). In addition, strain hardening of the alloy did not suggest the development of the TRIP effect during tension. In contrast, the impressive mechanical properties of the cold-rolled alloy (Fig. 3a, Table 2) and the strain hardening curve with a secondary peak at $\varepsilon \sim 0.1$ (Fig. 3d) suggested the development of a deformation-induced martensitic transformation (for example [1]) during tensile test at −196 °C. An increased work-hardening rate suppressed necking, thereby enhancing both the maximum strength and ductility.

Although both these conditions (as-cast and cold-rolled) showed an almost complete martensitic structure after tension at cryogenic temperature (Fig. 5), it seemed that this fcc-to-bcc transformation was associated with different mechanisms. Less obvious deformation-induced martensitic transformation in the as-cast condition suggests that the majority of martensite was formed *during cooling*, and a relatively small fraction of the bcc phase was caused by deformation. In contrast, in the cold-rolled condition, the majority of martensite was formed *during deformation*, thereby providing an obvious TRIP effect with a typical secondary peak in the strain hardening curve (Fig. 3d).

More intensive martensite transformation in the pre-strained alloy in comparison with the as-cast condition could be associated with the increased thermal stability of the fcc phase due to deformation-induced microstructure refinement. It has been reported for a number of steels that fine austenite usually exhibits a lower M_s temperature and enhanced thermal stability in comparison with coarse austenite [16, 26–29]. This effect is usually associated with an increased nonchemical driving force (i.e., elastic strain energy) for martensitic transformation due to structural refinement [25,26,30–32].

Meanwhile, pre-straining obviously influenced the strength of the alloy. The yield strength of the cold-rolled alloy is almost the same at room and cryogenic temperatures (1385 and 1380 MPa, respectively), and this high level of strength was provided by substructure strengthening (high dislocation density) and, sometimes, by interface strengthening due to the martensite formation (Fig. 2b, Table 2).

To evaluate the obtained mechanical properties under cryogenic conditions, the program alloy was compared with twinning-induced plasticity (TWIP) steels [33,34], austenitic stainless steels [32], and early studied HEA/MEAs [3,8,35–38] (Fig. 6). This schematic representation of the strength – ductility relationship showed a considerably higher ultimate tensile strength of the cold-rolled $Fe_{65}(CoNi)_{25}Cr_{9.5}C_{0.5}$ alloy without substantial loss in total elongation in comparison with the reference alloys. It is worth noting that materials possessing the TRIP effect do not often show very large ductility, particularly at cryogenic temperatures. Values of up to 70% of tensile elongation were attained by only some classes of TRIP steels [for example, [34,39]. The lower stability of austenite in the sub-zero interval [39,40] usually results in a massive martensite transformation at the very beginning of strain, because the TRIP effect does not contribute effectively to the enhancement of ductility. In our case, pre-straining (80% CR) shifted the martensitic transformation to larger strains, thereby increasing the ductility in comparison with the as-cast condition. In addition, some enhancement in both strength and ductility can be expected due to interface strengthening via the formation of fcc-bcc interfaces, which can have a coherent, semi-coherent or incoherent structure [1]. The combination of different mechanisms and timely switching provide promising properties. In addition, the obtained results suggested the feasibility of this strategy for the development of cryogenic HEAs/MEAs.

It is worth noting that the addition of carbon could also result in an increase in strength. Due to existing at a relatively low fraction (0.5 at. %) carbon did not formed carbides in the as cast condition, nor after deformation. Therefore, the main strengthening effect of C was associated with solid-solution hardening. The effect of C on the strength of stainless steel or TWIP steel was found to be 46 MPa/at %C and 76.6 MPa/at %C, respectively [42,43]. In CoCrFeMnNi-type HEAs, the contribution of carbon to strength was estimated to be 65–67 MPa/at % C [2,44]. It should be noted, however, that a much higher carbon-induced solid solution strengthening effect (178 MPa/at %C) was reported at room temperature for a $Fe_{40.4}Ni_{11.3}Mn_{34.8}Al_{7.5}Cr_6$ alloy [11]. In some HEAs (e.g., $CoCr_{0.25}FeMnNi$), this effect increased considerably at cryogenic temperatures, attaining 147 MPa/at %C at −196 °C in comparison with 67 MPa/at %C at room temperature [2].

The yield strength of $Fe_{65}Co_{10}Ni_{10}Cr_{15}$ in recrystallized conditions was found to be 330 and 535 MPa at room and cryogenic temperatures, respectively [6]. These values were noticeably higher than those obtained for the program alloy, even strengthened by interstitials. Since the effect of grain size on strength in high-entropy alloys is usually very high [8,11,45], it can be suggested that the observed difference was caused by a smaller average grain size (4 μm) compared to the as-cast structure in our case.

5. Conclusions

The structure and mechanical properties of a new medium-entropy $Fe_{65}(CoNi)_{25}Cr_{9.5}C_{0.5}$ alloy were investigated both at room and liquid nitrogen temperatures in the as-cast condition and after cold rolling to an 80% thickness reduction. The main findings are summarized as follows:

1. At −196 °C, the cold-rolled program alloy exhibited a combination of very high strength ($\sigma_{0.2}$ = 1360 MPa, σ_{UTS} = 2070 MPa), good ductility (δ = 26%) and excellent fracture toughness (approximately 700 kJ/m^2)
2. The obtained mechanical properties were associated with the superposition of deformation-induced fcc-to-bcc martensite phase transformation (and corresponding interface strengthening, which could also contribute to ductility), substructure strengthening, and solid solution strengthening. The better mechanical properties of the cold-rolled alloy at cryogenic temperatures, in comparison with the as-cast condition, could be associated with the increased thermal stability of the fcc phase due to deformation-induced microstructure refinement and shifting of the main martensite transformation to later stages of strain.

CRediT authorship contribution statement

E. Povolyaeva: Data curation, Investigation, Validation, Writing – original draft. S. Mironov: Validation, Writing – review & editing. D. Shaysultanov: Investigation, Validation, Visualization, Supervision, Project administration, Funding acquisition. N. Stepanov: Writing – review & editing. S. Zherebtsov: Methodology, Supervision, Writing – review & editing.

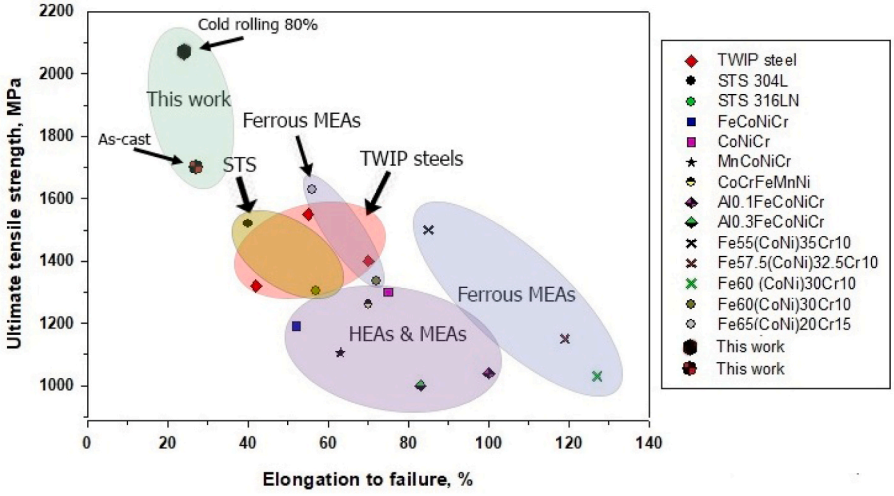

Fig. 6. Schematic representation of the strength – ductility relationship at liquid nitrogen temperature for the program alloy in comparison with various groups of HEAs/MEAs and steels shown earlier in Ref. [1] for $Fe_x(CoNi)_{90-x}Cr_{10}$ (x = 55, 57.5, and 60) alloys. Mechanical properties of other listed alloys were examined in Refs. [3,6,8,32–39,41].

Data availability statement

The raw/processed data required to reproduce these findings are available on request from the corresponding author.

Declaration of competing interest

The authors declare that they have no known competing financial interests or personal relationships that could have appeared to influence the work reported in this paper.

Acknowledgement

Financial support from the Russian Science Foundation (Grant No. 20-79-10093) is gratefully acknowledged. This work was carried out using equipment of the Joint Research Center of Belgorod State National Research University « Technology and Materials».

Appendix A. Supplementary data

Supplementary data to this article can be found online at https://doi.org/10.1016/j.msea.2022.142720.

References

[1] J.W. Bae, J.B. Seol, J. Moon, S.S. Sohn, M.J. Jang, H.Y. Um, B.-J. Lee, H.S. Kim, Exceptional phase-transformation strengthening of ferrous medium-entropy alloys at cryogenic temperatures, Acta Mater. 161 (2018) 388–399, https://doi.org/10.1016/j.actamat.2018.09.057.
[2] M.V. Klimova, A.O. Semenyuk, D.G. Shaysultanov, G.A. Salishchev, S. V. Zherebtsov, N.D. Stepanov, Effect of carbon on cryogenic tensile behavior of CoCrFeMnNi-type high entropy alloys, J. Alloys Compd. 811 (2019) 152000, https://doi.org/10.1016/j.jallcom.2019.152000.
[3] Z. Wu, H. Bei, G.M. Pharr, E.P. George, Temperature dependence of the mechanical properties of equiatomic solid solution alloys with face-centered cubic crystal structures, Acta Mater. 81 (2014) 428–441, https://doi.org/10.1016/j.actamat.2014.08.026.
[4] M. Klimova, D. Shaysultanov, A. Semenyuk, S. Zherebtsov, G. Salishchev, N. Stepanov, Effect of nitrogen on mechanical properties of CoCrFeMnNi high entropy alloy at room and cryogenic temperatures, J. Alloys Compd. 849 (2020) 156633, https://doi.org/10.1016/j.jallcom.2020.156633.
[5] J. Lee, J. Moon, J.W. Bae, J.M. Park, H. Kwon, H. Kato, H.S. Kim, Temperature- and strain-dependent thermally-activated deformation mechanism of a ferrous medium-entropy alloy, Intermetallics 134 (2021) 107202, https://doi.org/10.1016/j.intermet.2021.107202.
[6] K. Zhang, X. Zhang, E. Zhang, R. Wei, L. Wang, J. Chen, S. Yuan, Z. Han, C. Chen, F. Li, Strengthening of ferrous medium entropy alloys by promoting phase transformation, Intermetallics 136 (2021) 107265, https://doi.org/10.1016/j.intermet.2021.107265.
[7] F. Haftlang, P. Asghari-Rad, J. Moon, A. Zargaran, K.-A. Lee, S.-J. Hong, H.S. Kim, Simultaneous effects of deformation-induced plasticity and precipitation hardening in metastable non-equiatomic FeNiCoMnTiSi ferrous medium-entropy alloy at room and liquid nitrogen temperatures, Scripta Mater. 202 (2021) 114013, https://doi.org/10.1016/j.scriptamat.2021.114013.
[8] F. Otto, A. Dlouhý, C. Somsen, H. Bei, G. Eggeler, E.P. George, The influences of temperature and microstructure on the tensile properties of a CoCrFeMnNi high-entropy alloy, Acta Mater. 61 (2013) 5743–5755, https://doi.org/10.1016/j.actamat.2013.06.018.
[9] N. Stepanov, M. Tikhonovsky, N. Yurchenko, D. Zyabkin, M. Klimova, S. Zherebtsov, A. Efimov, G. Salishchev, Effect of cryo-deformation on structure and properties of CoCrFeNiMn high-entropy alloy, Intermetallics 59 (2015) 8–17, https://doi.org/10.1016/j.intermet.2014.12.004.
[10] Z. Li, K.G. Pradeep, Y. Deng, D. Raabe, C.C. Tasan, Metastable high-entropy dual-phase alloys overcome the strength-ductility trade-off, Nature 534 (2016) 227–230, https://doi.org/10.1038/nature17981.
[11] Z. Wang, I. Baker, W. Guo, J.D. Poplawsky, The effect of carbon on the microstructures, mechanical properties, and deformation mechanisms of thermo-mechanically treated Fe40.4Ni11.3Mn34.8Al7.5Cr6 high entropy alloys, Acta Mater. 126 (2017) 346–360, https://doi.org/10.1016/j.actamat.2016.12.074.
[12] Z. Li, Interstitial equiatomic CoCrFeMnNi high-entropy alloys: carbon content, microstructure, and compositional homogeneity effects on deformation behavior, Acta Mater. 164 (2019) 400–412, https://doi.org/10.1016/j.actamat.2018.10.050.
[13] N.D. Stepanov, N.Y. Yurchenko, M.A. Tikhonovsky, G.A. Salishchev, Effect of carbon content and annealing on structure and hardness of the CoCrFeNiMn-based high entropy alloys, J. Alloys Compd. 687 (2016) 59–71, https://doi.org/10.1016/j.jallcom.2016.06.103.
[14] Z. Li, C.C. Tasan, K.G. Pradeep, D. Raabe, A TRIP-assisted dual-phase high-entropy alloy: grain size and phase fraction effects on deformation behavior, Acta Mater. 131 (2017) 323–335, https://doi.org/10.1016/j.actamat.2017.03.069.
[15] S.S. Nene, M. Frank, K. Liu, R.S. Mishra, B.A. McWilliams, K.C. Cho, Extremely high strength and work hardening ability in a metastable high entropy alloy, Sci. Rep. 8 (2018) 9920, https://doi.org/10.1038/s41598-018-28383-0.
[16] G.B. Olson, M. Azrin, Transformation behavior of TRIP steels, Metall. Trans. A 9 (1978) 713–721, https://doi.org/10.1007/BF02659928.
[17] F. Haftlang, H.S. Kim, A perspective on precipitation-hardening high-entropy alloys fabricated by additive manufacturing, Mater. Des. 211 (2021) 110161, https://doi.org/10.1016/j.matdes.2021.110161.
[18] D. Ma, M. Yao, K.G. Pradeep, C.C. Tasan, H. Springer, D. Raabe, Phase stability of non-equiatomic CoCrFeMnNi high entropy alloys, Acta Mater. 98 (2015) 288–296, https://doi.org/10.1016/j.actamat.2015.07.030.
[19] A. Shibata, H. Yonezawa, K. Yabuuchi, S. Morito, T. Furuhara, T. Maki, Relation between martensite morphology and volume change accompanying fcc to bcc martensitic transformation in Fe–Ni–Co alloys, Mater. Sci. Eng. 438–440 (2006) 241–245, https://doi.org/10.1016/j.msea.2005.12.044.
[20] A. Belyakov, Y. Kimura, K. Tsuzaki, Microstructure evolution in dual-phase stainless steel during severe deformation, Acta Mater. 54 (2006) 2521–2532, https://doi.org/10.1016/j.actamat.2006.01.035.
[21] Y. He, S. Godet, J.J. Jonas, Observations of the Gibeon meteorite and the inverse Greninger–Troiano orientation relationship, J. Appl. Crystallogr. 39 (2006) 72–81, https://doi.org/10.1107/S0021889805038276.
[22] L.D. Jaffe, J.H. Hollomon, Hardenability and quench cracking, Trans. AIME 167 (1946) 617–646.
[23] J. Kobayashi, D. Ina, N. Yoshikawa, K.I. Sugimoto, Effects of the addition of Cr, Mo and Ni on the microstructure and retained austenite characteristics of 0.2% C-Si-Mn-Nb ultrahigh-strength TRIP-aided bainitic ferrite steels, ISIJ Int. 52 (2012) 1894–1901, https://doi.org/10.2355/isijinternational.52.1894.
[24] L.F. Alvarez, C. Garcia, V. Lopez, Continuous cooling transformations in martensitic stainless steels, ISIJ Int. 34 (1994) 516–521, https://doi.org/10.2355/isijinternational.34.516.
[25] Y. Li, D.S. Martín, J. Wang, C. Wang, W. Xu, A review of the thermal stability of metastable austenite in steels: martensite formation, J. Mater. Sci. Technol. 91 (2021) 200–214, https://doi.org/10.1016/j.jmst.2021.03.020.
[26] S. Takaki, K. Fukunaga, J. Syarif, T. Tsuchiyama, Effect of grain refinement on thermal stability of metastable Austenitic steel, Mater. Trans. 45 (2004) 2245–2251, https://doi.org/10.2320/matertrans.45.2245.
[27] Y. Matsuoka, T. Iwasaki, N. Nakada, T. Tsuchiyama, S. Takaki, Effect of grain size on thermal and mechanical stability of austenite in metastable Austenitic stainless steel, ISIJ Int. 53 (2013) 1224–1230, https://doi.org/10.2355/isijinternational.53.1224.
[28] H.S. Yang, H.K.D.H. Bhadeshia, Austenite grain size and the martensite-start temperature, Scripta Mater. 60 (2009) 493–495, https://doi.org/10.1016/j.scriptamat.2008.11.043.
[29] A. García-Junceda, C. Capdevila, F.G. Caballero, C.G. de Andrés, Dependence of martensite start temperature on fine austenite grain size, Scripta Mater. 58 (2008) 134–137, https://doi.org/10.1016/j.scriptamat.2007.09.017.
[30] Z.H. Cai, H. Ding, R.D.K. Misra, Z.Y. Ying, Austenite stability and deformation behavior in a cold-rolled transformation-induced plasticity steel with medium manganese content, Acta Mater. 84 (2015) 229–236, https://doi.org/10.1016/j.actamat.2014.10.052.
[31] W.X. Zhang, Y.Z. Chen, Y.B. Cong, Y.H. Liu, F. Liu, On the austenite stability of cryogenic Ni steels: microstructural effects: a review, J. Mater. Sci. 56 (2021) 12539–12558, https://doi.org/10.1007/s10853-021-06068-w.
[32] P. Czarkowski, A.T. Krawczyńska, T. Brynk, M. Nowacki, M. Lewandowska, K. J. Kurzydłowski, Cryogenic strength and microstructure of a hydrostatically extruded austenitic steel 1.4429 (AISI 316LN), Cryogenics 64 (2014) 1–4, https://doi.org/10.1016/j.cryogenics.2014.07.014.
[33] D.T. Read, R.P. Reed, Fracture and strength properties of selected austenitic stainless steels at cryogenic temperatures, Cryogenics 21 (1981) 415–417, https://doi.org/10.1016/0011-2275(81)90175-2.
[34] S.S. Sohn, S. Hong, J. Lee, B.C. Suh, S.K. Kim, B.J. Lee, N.J. Kim, S. Lee, Effects of Mn and Al contents on cryogenic-temperature tensile and Charpy impact properties in four austenitic high-Mn steels, Acta Mater. 100 (2015) 39–52, https://doi.org/10.1016/j.actamat.2015.08.027.
[35] B. Gludovatz, A. Hohenwarter, D. Catoor, E.H. Chang, E.P. George, R.O. Ritchie, A fracture-resistant high-entropy alloy for cryogenic applications, Science (80) 345 (2014) 1153–1158, https://doi.org/10.1126/science.1254581.
[36] B. Gludovatz, A. Hohenwarter, K.V.S. Thurston, H. Bei, Z. Wu, E.P. George, R. O. Ritchie, Exceptional damage-tolerance of a medium-entropy alloy CrCoNi at cryogenic temperatures, Nat. Commun. 7 (2016) 10602, https://doi.org/10.1038/ncomms10602.
[37] A. Gali, E.P. George, Tensile properties of high- and medium-entropy alloys, Intermetallics 39 (2013) 74–78, https://doi.org/10.1016/j.intermet.2013.03.018.
[38] D. Li, Y. Zhang, The ultrahigh charpy impact toughness of forged AlxCoCrFeNi high entropy alloys at room and cryogenic temperatures, Intermetallics 70 (2016) 24–28, https://doi.org/10.1016/j.intermet.2015.11.002.
[39] M. Soleimani, A. Kalhor, H. Mirzadeh, Transformation-induced plasticity (TRIP) in advanced steels: a review, Mater. Sci. Eng. 795 (2020) 140023, https://doi.org/10.1016/j.msea.2020.140023.
[40] L. Wang, J.G. Speer, Quenching and partitioning steel heat treatment, Metallogr. Microstruct. Anal. 2 (2013) 268–281, https://doi.org/10.1007/s13632-013-0082-8.

[41] L. Smith, B. Craig, Properties of metallic materials for LNG service, Stainl. Steel World 13 (2001) 27–32.
[42] Valentin G. Gavriljuk, Hans Berns, Berns, High Nitrogen Steels, Springer Berlin Heidelberg, Berlin, Heidelberg, 1999, https://doi.org/10.1007/978-3-662-03760-7.
[43] O. Bouaziz, H. Zurob, B. Chehab, J.D. Embury, S. Allain, M. Huang, Effect of chemical composition on work hardening of Fe-Mn-C TWIP steels, Mater. Sci. Technol. 27 (2011) 707–709, https://doi.org/10.1179/026708309X12535382371852.
[44] J. Chen, Z. Yao, X. Wang, Y. Lu, X. Wang, Y. Liu, X. Fan, Effect of C content on microstructure and tensile properties of as-cast CoCrFeMnNi high entropy alloy, Mater. Chem. Phys. 210 (2018) 136–145, https://doi.org/10.1016/j.matchemphys.2017.08.011.
[45] S.J. Sun, Y.Z. Tian, H.R. Lin, X.G. Dong, Y.H. Wang, Z.J. Wang, Z.F. Zhang, Temperature dependence of the Hall–Petch relationship in CoCrFeMnNi high-entropy alloy, J. Alloys Compd. 806 (2019) 992–998, https://doi.org/10.1016/j.jallcom.2019.07.357.